JPE 11-2-5

Extending Switching Frequency for Torque Ripple Reduction Utilizing a Constant Frequency Torque Controller in DTC of Induction Motors

Auzani Jidin†, Nik Rumzi Nik Idris *, Abdul Halim Mohd Yatim*, Tole Sutikno**, and Malik E. Elbuluk***

† Dept. of Power Electronics and Drives, FKE, Universiti Teknikal Malaysia Melaka, Malaysia
* Dept. of Energy Conversion, FKE, Universiti Teknologi Malaysia, Malaysia
** Dept. of Electrical Engineering, Universitas Ahmad Dahlan, Indonesia
*** Dept. of Electrical Engineering, University of Akron, USA

Abstract

Direct torque control (DTC) of induction machines is known to offer fast instantaneous torque and flux control with a simple control structure. However, this scheme has two major disadvantageous, namely, a variable inverter switching frequency and a high torque ripple. These problems occur due to the use of hysteresis comparators in conventional DTC schemes, particularly in controlling the output torque. This paper reviews the utilization of constant frequency torque controllers (CFTC) in DTC to solve these problems while retaining the simple control structure of DTC. Some extensions of the work in utilizing a CFTC will be carried out in this paper which can further reduce the torque ripple. This is particularly useful for a system which has a limited/low sampling frequency. The feasibility of a CFTC with an extended carrier frequency in minimizing the torque ripple is verified through experimental results.

Key Words: Direct Torque Control, Induction Machine, Switching Frequency, Torque Ripple Reduction

I. INTRODUCTION

The direct torque control (DTC) of induction motor drives has gained popularity in advanced motor drive applications since it offers fast instantaneous torque and flux control with simple implementation. This scheme is well known for its robustness in control as it is less dependent on machine parameters, does not require a complex field orientation block, a speed encoder and an inner current regulation loop. However, this scheme, which is based on hysteresis comparators [1], has major drawbacks namely a variable switching frequency, a large torque ripple and high sampling requirements for digital implementation.

It makes sense that a reduction in output torque ripple can be achieved when a lower band of torque hysteresis is used in order to restrict the ripple within the band. However, this cannot be realized using a microprocessor or a digital signal processor, particularly when an extreme torque slope occurs with an inappropriate band level (which is too small). Ideally, hysteresis-based operation is suitable for a discrete system which has a fast processor such that the bang-bang control can be performed the same as in analog operation. Instead of lowering the hysteresis band with a fast processor, one can inject high-frequency triangular waveforms into the errors in torque and flux [2]. This method is called the dithering technique, and it is simple and effective in minimizing torque ripple. However, it still produces an unpredictable switching frequency since the torque slopes that determine the frequency of the torque controller vary depending on the operating conditions [3], [4].

Several methods have been proposed to overcome this problem (i.e. an unpredictable switching frequency) [5]-[15]. With consideration of the variations in torque slope, a constant switching frequency can be provided when the hysteresis bands themselves are adjusted according to operating conditions [5]. The adjustability of hysteresis bands is established based on a PI controller and a pulse counter for each of the torque and flux controllers. This, consequently, increases the complexity of the DTC drive. Moreover, this technique does not guarantee a reduction in torque ripple as it the case with hysteresis-based controllers. To eliminate the inherent problems of hysteresis-based controllers, it is possible to determine an optimal switching instant for each of the switching cycles that satisfies the minimum-torque ripple condition [7]-[9]. In this case, the term called a duty ratio is determined

Manuscript received Sep. 24, 2010; revised Jan. 30, 2011
† Corresponding Author: auzani@utem.edu.my
Tel: +606-555-2345, Fax: +606-555-2226/2222, UTeM
† Dept. of Power Electronics and Drives, FKE, Universiti Teknikal Malaysia Melaka (UTeM), Malaysia
* Dept. of Energy Conversion, FKE, Universiti Teknologi Malaysia (UTM), Malaysia
** Dept. of Electrical Engineering, Universitas Ahmad Dahlan (UAD), Indonesia
*** Dept. of Electrical Engineering, University of Akron, USA

so that an appropriate active state is switched for some portion of a switching period, and the zero vector is selected for the rest of the period. Another method, which is very popular in solving these problems is the use of space vector modulation [6],[10],[13]-[15]. In this approach, a switching period is subdivided into three or more states, to synthesize a desired voltage vector in order to produce the minimum torque ripple. In both approaches, the application of a fast processor to compute the duty ratio or the voltage vectors for every switching period is necessary, particularly when a small sampling time is required.

Recently, the use of predictive control methods in hysteresis-based DTC has gained a considerable amount of attention, particularly due to its ability to reduce the torque ripple and as well as the switching frequency [16]-[18]. Although, a reduced torque ripple is achieved, the switching frequency still varies, since it depends on the operating conditions as well as the possible applied voltage vectors.

This paper reviews the use of constant frequency torque controllers (CFTC) in the direct torque control (DTC) of induction machines to reduce the output torque ripple with a constant switching frequency as proposed in [11]. However, it is possible to further increase the switching frequency in [11] which will result in a further reduction of the torque ripple, particularly when DTC is performed with a limited sampling frequency, i.e. a low speed processor. Some extensions of the work in utilizing CFTC in DTC will be highlighted in this paper to show that:

1) A high switching frequency to further reduce the output torque ripple can be established with a CFTC, by extending the triangular carrier frequency up to one-quarter of the maximum sampling frequency achieved by a DSP.
2) With suitable PI-controller gains, excellent control of the output torque as well as a significant reduction in the torque ripple can be achieved at the maximum triangular carrier frequency. A simple linear relationship between the input-output of the triangular carrier model (as obtained in [11]) can still be assumed and the output torque can still be regulated if an appropriate cross-over frequency is selected based on the maximum switching frequency.

An extension of the constant switching frequency is particularly useful for a system which has a limited/low sampling frequency. Moreover, this paper also presents a quick guide for the design of CFTC to simplify the detailed description in [11]. The feasibility of the use of a CFTC in DTC in reducing torque ripple (at three different carrier frequencies) is verified through experimentation as well as a comparison with a conventional DTC scheme. In section II of this paper, the basic principle of DTC is briefly discussed. DTC with a CFTC is briefly explained in Section III. Section IV presents a quick guide of the design procedures for a CFTC in DTC. Section V presents the implementation and experimental results of a CFTC in DTC. Finally the conclusions are given in Section VI.

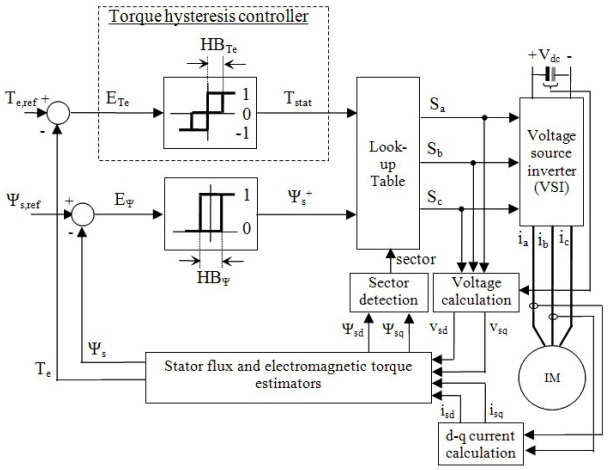

Fig. 1. Structure of basic DTC-hysteresis based induction machine.

II. Basic Principle of DTC

The behavior of induction machines in DTC drives can be described in terms of space vectors by the following equations written in the stator stationary reference frame:

$$v_s = r_s i_s + \frac{d\psi_s}{dt} \tag{1}$$

$$0 = r_r i_r - j\omega_r \psi_r + \frac{d\psi_r}{dt} \tag{2}$$

$$\psi_s = L_s i_s + L_m i_r \tag{3}$$

$$\psi_r = L_r i_r + L_m i_s \tag{4}$$

$$T_e = \frac{3}{2} P |\psi_s||i_s| \sin\delta \tag{5}$$

where P is the number of pole pairs, ω_r is the rotor electric angular speed in rad./s, L_s, L_r and L_m are the motor inductances and δ is the angle between the stator flux linkage and the stator current space vectors. Based on (1) the d^s- and q^s-axis stator flux in the stationary reference frame can be written as:

$$\psi_{s,d}{}^s = \int (v_{s,d}{}^s - i_{s,d}{}^s r_s) dt \tag{6a}$$

$$\psi_{s,q}{}^s = \int (v_{s,q}{}^s - i_{s,q}{}^s r_s) dt. \tag{6b}$$

In terms of the switching states S_a, S_b, and S_c (which can be either 0 or 1) the voltage vectors in (6) are given by:

$$v_{s,d}{}^s = \frac{1}{3} V_{dc} (2S_a - S_b - S_c) \tag{7a}$$

$$v_{s,q}{}^s = \frac{1}{\sqrt{3}} V_{dc} (S_b - S_c). \tag{7b}$$

The electromagnetic torque given in (5) can be rewritten in the d^s-q^s coordinates as:

$$T_e = \frac{3}{2} P (\psi_{s,d}{}^s i_{s,q}{}^s - \psi_{s,q}{}^s i_{s,d}{}^s). \tag{8}$$

Fig. 1 shows the structure of the DTC hysteresis-based control as initially proposed by [1]. The output stator voltage is applied based on the selection of the switching states (S_a, S_b, S_c) from a look-up table. These switching states are selected based on whether the torque and the stator flux need to be

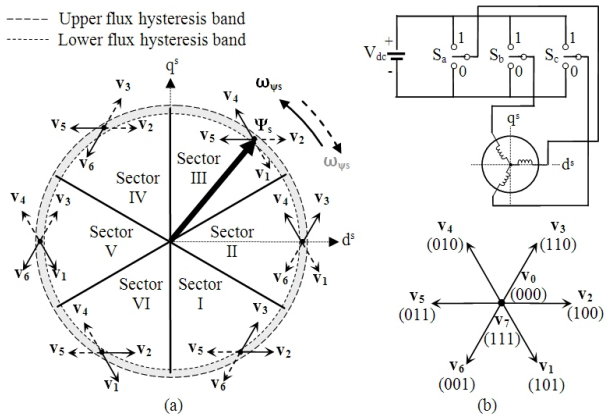

Fig. 2. Selection of the optimum inverter output voltage vectors. (a) Each sector indicates the appropriate voltage vectors. (b) Eight possible switches configuration in the three-phase VSI.

TABLE I
LOOK-UP TABLE (VOLTAGE VECTOR SELECTION)

Stator flux error status, ψ_s^+	Torque error status, T_{stat}	Sec. I	Sec. II	Sec. III	Sec. IV	Sec. V	Sec. VI
1	1	V_2 (100)	V_3 (110)	V_4 (010)	V_5 (011)	V_6 (001)	V_1 (101)
	0	V_0 (000)	V_7 (111)	V_0 (000)	V_7 (111)	V_0 (000)	V_7 (111)
	-1	V_6 (001)	V_1 (101)	V_2 (100)	V_3 (110)	V_4 (010)	V_5 (011)
0	1	V_3 (110)	V_4 (010)	V_5 (011)	V_6 (001)	V_1 (101)	V_2 (100)
	0	V_7 (111)	V_0 (000)	V_7 (111)	V_0 (000)	V_7 (111)	V_0 (000)
	-1	V_5 (011)	V_6 (001)	V_1 (101)	V_2 (100)	V_3 (110)	V_4 (101)

increased or decreased and also on the stator flux position. The decisions as to whether the torque and/or the flux need to be increased or decreased comes from the three-level and two-level hysteresis comparators for the torque and stator flux, respectively. Fig. 2 illustrates the two optimized voltage vectors in every sector, which are selected from the eight possible switch configurations, using the look-up table given in Table I [1].

Notice that in order to control the flux, two active voltage vectors are required. On the other hand, to control the torque, one active voltage vector is used to increase the torque while a zero voltage vector is used to reduce it. By limiting the torque and flux errors to within their hysteresis bands, a de-coupled control of the torque and flux is achieved.

It is well-known that the main drawbacks of hysteresis-based DTC schemes are their variable inverter switching frequency, high sampling requirement for digital implementation and high torque ripple. To highlight these problems, some experimental results showing output torque ripples obtained in hysteresis-based DTC at different applied sampling frequencies and/or torque hysteresis bands are presented as shown in Fig. 3.

For each case, the control of the torque at 6 Nm was performed under the same load torque condition so that the rotor speed operated at around 400 rpm. The nominal level of the torque hysteresis band is HB_{Te} (0.9 Nm) and the minimum sampling time achievable using DSP is DT (55μs) (more

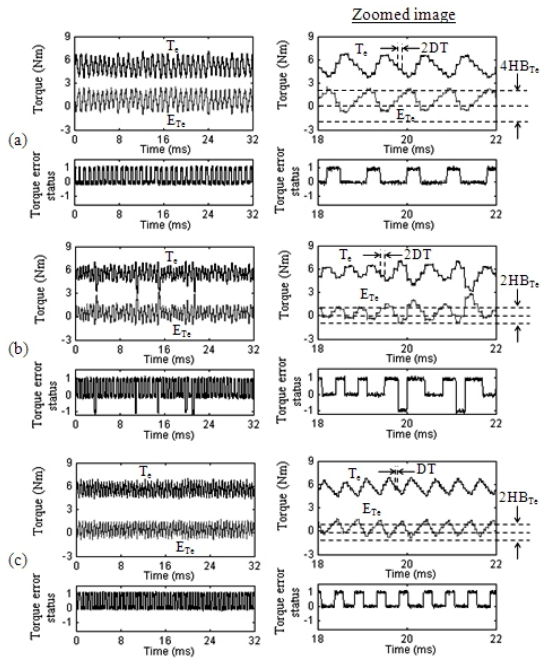

Fig. 3. Experimental results of control of output torque utilizing three-level hysteresis comparator (in hysteresis based-DTC). (a) Hysteresis band = $2HB_{Te}$, sampling time=2DT, (b) hysteresis band = HB_{Te}, sampling time=DT.

information on the values of the machine and the control system parameters will be presented in Section V). From Fig. 3(a), as expected, the output torque ripple is high when the torque hysteresis band is set to twice the HB_{Te}. Thus, the torque ripple of the hysteresis-based DTC can be reduced by reducing the hysteresis band. Fig. 3(b) shows the results of the output torque control when the torque hysteresis band reduces to HB_{Te}. However, due to the sampling time used in Fig. 3(b) (and also in Fig. 3(a)) it is twice of the nominal DT (i.e. 110μs). This leads to incorrect voltage vector selections (where $T_{stat} = -1$) which cause rapid decreases in the output torque and hence increases in the torque ripple, as can be seen in Fig. 3(b). Therefore, to eliminate the incorrect voltage vector selections, the sampling time needs to be reduced, as demonstrated in Fig. 3(c) whereby the sampling is set to DT. As can be seen in Fig. 3(c), the output torque ripple is decreased and no active voltage vector is selected to reduce the torque.

III. DTC WITH CONSTANT FREQUENCY TORQUE CONTROLLER

An attempt has been made to provide a constant switching frequency and reduced the torque ripple in DTC by replacing the torque hysteresis controller with a constant frequency torque controller (CFTC) as depicted in Fig. 4 [11]. The constant frequency torque controller (as shown in Fig. 4) consists of two triangular generators, two comparators and a proportional-integral (PI) controller. In principle, the function of the torque error status T_{stat} generated from the CFTC is similar to that of a three-level hysteresis comparator [1], which can be in one of three states; -1, 0 or 1. Note that, no modification of the original look-up table is required. As a result, the decouple control structure as well as the simple control structure of hysteresis-based DTC can be retained.

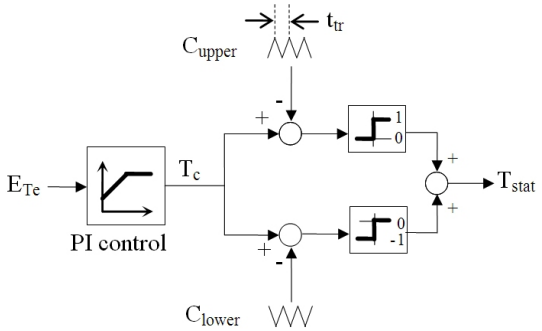

Fig. 4. Constant frequency torque controller (CFTC).

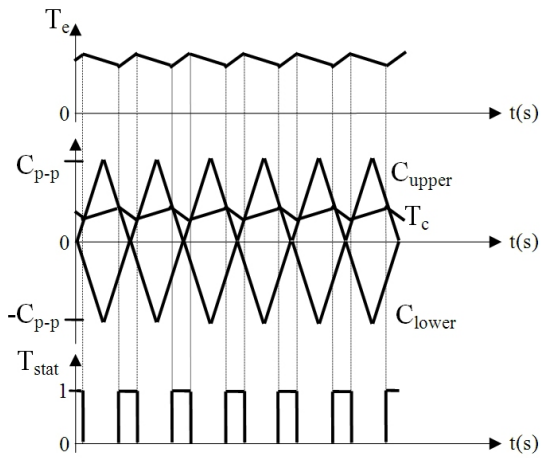

Fig. 5. Typical waveforms of the constant frequency torque controller.

Fig. 5 shows the typical waveforms of a constant frequency torque controller. The torque error status T_{stat} generated from the constant frequency torque controller can be described by the following equation:

$$T_{stat} = \begin{cases} 1 & \text{for} \quad T_c \geq C_{\text{upper}} \\ 0 & \text{for} \quad C_{\text{lower}} < T_c < C_{\text{upper}} \\ -1 & \text{for} \quad T_c \leq C_{\text{lower}} \end{cases} \tag{9}$$

where T_c is output of proportional-integral (PI) control while C_{upper} and C_{lower} are the upper and lower triangular waveforms, respectively. Note that, the two triangular waveforms (C_{upper} and C_{lower}) are 180° out of phase with each other. In order to establish a constant switching frequency, the frequency and peak to peak of the upper and lower triangular waveforms are set to fixed values. It is desirable to set a high triangular waveform frequency in minimizing the output torque ripple. For a PI torque controller, the gain values of K_p and K_i are restricted to ensure that the absolute slope of the output signal, T_c does not exceed the absolute slope of the triangular waveform. This is to ensure the proper operation of the torque control at a constant switching frequency and to avoid the selection of incorrect voltage vectors, for a wide range of operating conditions.

IV. Design Procedure for a Constant Frequency Torque Controller in DTC

This section presents a quick guide to designing a proper constant frequency torque controller in the DTC of induction machines. Briefly, there are three steps to obtaining the proper

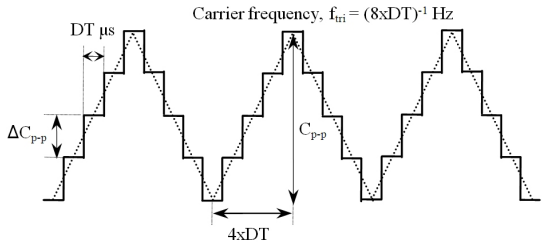

Fig. 6. Generated upper triangular waveform using DSP (sampled at DT μs).

operation of a CFTC. A detailed explanation on how the related equations (as shown later) were derived and how some of the assumptions made, can be found in [11].

Step 1: Select an appropriate frequency for the triangular waveforms

It is desirable to have a large triangular frequency in order to acquire a large torque loop bandwidth and hence a faster torque response. Moreover, with a higher triangular frequency the output torque ripple will be reduced. The triangular waveforms are generated by software sampled at the maximum sampling rate to execute the algorithms (i.e DTC including a CFTC) but limited by the DSP speed. For example, the upper triangular waveform produced by the DSP is depicted in Fig. 6, whereby DT is the sampling period of the DSP. In this particular example, a complete triangular waveform is completed in a DSP sampling time of eight.

Step 2: Determine the gain value of K_p

It must be ensured that the absolute slope of T_c does not exceed the absolute slope of the triangular waveforms, which are mainly determined by the proportional gain (K_p) of the PI controller. The absolute slope of the triangular waveform (as shown in Fig. 6) can be simply obtained as:

$$\begin{aligned} &\text{<absolute slope of the triangular waveform>} \\ &\qquad = \left| \frac{C_{p-p}}{4DT} \right|. \end{aligned} \tag{10}$$

According to [10]; for a positive slope of Tc, the following condition must be satisfied:

$$\begin{aligned} &\text{<absolute slope of the triangular waveform>} \\ &\qquad \geq \left\{ -AT_e + BV_s^{\psi_s} + K_t \left(\frac{\omega_{\text{slip}}}{d} - \omega_r^+ \right) \right\} K_p^+ \end{aligned} \tag{11}$$

meanwhile, for a negative slope, the following condition must be satisfied:

$$\begin{aligned} &\text{<absolute slope of the triangular waveform>} \\ &\qquad \geq \left| -AT_e - K_1 \omega_r^- \right| K_p^- \end{aligned} \tag{12}$$

where,

$$A = \left(\frac{1}{\sigma \tau_s} + \frac{1}{\sigma \tau_r} \right) \tag{13}$$

$$B = \frac{6PL_M}{4\sigma L_s L_r} \psi_s \tag{14}$$

$$K_1 = \frac{3P}{2} \frac{L_m}{\sigma L_s L_r} (\psi_s \psi_r) \tag{15}$$

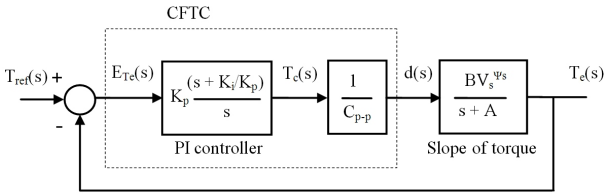

Fig. 7. Averaged and linearized torque loop (as in [11]).

$$d = \frac{AT_e - K_1\omega_{\text{slip}}}{BV_s^{\Psi_s}}. \tag{16}$$

In (13)-(15), σ is the total leakage factor, given by $(1 - L_m^2/(L_rL_s))$. τ_r and τ_s are the rotor and stator time constants, respectively. The term $V_s^{\Psi_s}$ (11) and (16) is the voltage vector magnitude, given by $(2V_{dc}/3)$.

It should be noted, that the occurrence of an extreme slope of T_c (either positive or negative slope) depends on the operating conditions. Considering that the motor operates under the worst-case conditions, (i.e. the torque and flux are operated under the rated conditions), it is therefore, according to (11) (or (12)), the maximum K_p^+ (or K_p^-) that limits the slope of T_c (or absolute slope of T_c) to its maximum. This is assumed to occur at a zero rotor speed (or at the base rotor speed) and at the rated slip. That is, $\omega_r^+ = 0$ for (11) and ω_r^- is set at the base speed for (12). Thus, to ensure proper operation the proportional gain (K_p) is obtained as:

$$K_p = \min\{K_p^+, K_p^-\}. \tag{17}$$

Step 3: Determine the gain value of K_i

Fig. 7 depicts a block diagram of the linearized torque loop proposed in [10]. The dashed box in Fig. 7 represents the constant frequency torque controller (CFTC). To select the gain constants of the PI controller in the torque loop, which results in a phase margin of 65° (or higher), the zero of the PI controller is chosen to be the same as the pole of the open-loop gain (or the pole in the torque slope transfer function). Under this condition, the integral gain K_i is calculated as:

$$K_i = K_pA. \tag{18}$$

In this way, an infinite dc gain due to the presence of an integrator in the PI controller will reduce the steady state error to zero. Based on the linear control theory, the obtained values for K_p and K_i (from (17) and (18)), must be adjusted such that the torque loop gain crossover frequency is much smaller than the carrier frequency. For a clearer picture, the determination of the PI controller's gain, presented in section V, will use numerical values based on the actual motor parameters given in Table II.

V. Implementation and Experimental Results

The feasibility of the CFTC in DTC, in providing a constant switching frequency and a reduced torque ripple has been realized with a complete drive system as shown in Fig. 8. The control algorithm is implemented on a DSPACE 1102 and an Altera FPGA (APEX20KE). Some of the main tasks of the DTC (i.e. the look-up table and the blanking time) are implemented utilizing the FPGA. As a result, the DSP (DSPACE 1102) is able to execute the DTC algorithm including the CFTC operation in the minimum sampling period which is 55 μs.

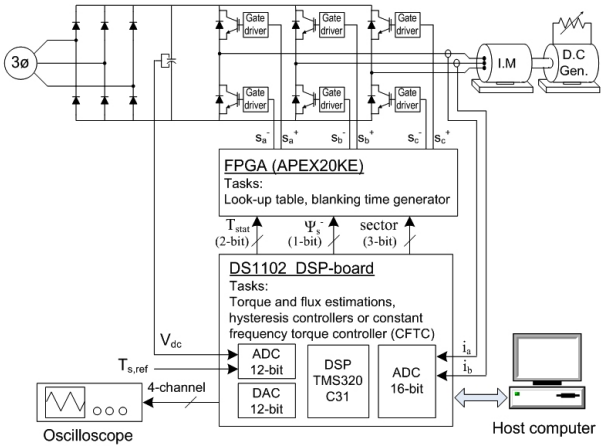

Fig. 8. Complete drive system of the experiment set-up.

Based on the previous discussion, in order to obtain the maximum reduction in the torque ripple, the switching frequency needs to be increased. Normally this can be achieved by using a high-speed DSP system. For example, the use of the SVM technique in DTC requires a fast processor to calculate the duty cycles or the voltage vectors for every sampling period. With a small sampling period, a reduction of the output torque ripple is accomplished since more switching states are applied within a switching period [6][10][13]-[15]. This paper, on the other hand, suggests a simple method for utilizing CFTC to extend the switching frequency. By using this method, an increase in the triangular frequency can be established without requiring a reduction in the sampling period of the DSP.

To verify this, a comparison of the output torque ripple obtained from three schemes was carried out; where each of schemes performed at three different 'triangular' frequencies but at the same sampling period, DT=55μs. For ease of identification, these schemes are referred as:

1) DTC-CSF1-DTC with CFTC at 2.2727 kHz,
2) DTC-CSF2 - DTC with CFTC at 3.0303 kHz,
3) DTC-CSF3 - DTC with CFTC at 4.5454 kHz.

The generated upper triangular waveforms for each scheme can be illustrated as depicted in Fig. 9. For example, if we consider the case of DTC-CSF1, eight steps per cycle of the triangular are used, that is for 100 units peak-peak the corresponding vertical resolution of the triangular waveform is 25 units per step, as can be seen in Fig. 9(a). From the figure, it can also be seen that the frequency of the triangular waveform is about 2.2727 kHz and the slope of the triangular is equal to 454545.45s^{-1}.

The actual parameters of an induction motor are shown in Table II. For safety reasons, the DC voltage was limited to 240V, which means that the base speed is reduced to 570 rpm. With the values of the machine parameters listed in Table II, the suitable values for K_p and K_i for each scheme, were determined as explained in section IV. The open-loop Bode plots with the PI controllers' gains for each scheme, are shown in Fig. 10. The gains for the PI controllers and the

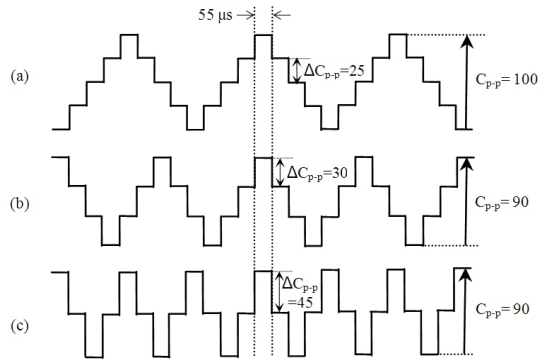

Fig. 9. Generated upper triangular waveforms sampled at 55 μs. (a) DTC-CSF1, (b) DTC-CSF2 and (c) DTC-CSF3.

TABLE II
INDUCTIONI MACHINE PARAMETERS.

Stator resistance	5.5 Ω
Rotor resistance	4.45 Ω
Stator self inductance	313.9 mH
Rotor self inductance	313.9 mH
Mutual inductance	299 mH
Number of poles	4
Stator flux rated	0.892 Wb
Torque rated	9 Nm
Voltage vector magnitude, $V_s^{\psi_s}$	160 V
Slip rated, ω_{slip}	9.4248
Base speed	570 rpm.

approximated crossover frequency (as shown in Fig. 9) for each scheme, are given in Table III.

Fig. 11 depicts the frequency spectrum of the phase current obtained from the experimental results for basic DTC, DTC-CSF1, DTC-CSF2 and DTC-CSF3 at speeds of 20 rad/s, 30 rad/s and 55 rad/s while the output torque was controlled to 2 Nm. It can be seen that the phase currents in schemes for DTC with CFTC (i.e. DTC-CSF1, DTC-CSF2 and DTC-CSF3) contains dominant harmonics at their respective triangular frequencies regardless of speed, unlike the hysteresis-based DTC which has a frequency spectrum that is spread out and depends on the operating speed. From this figure, it can also be seen that, a higher torque is obtained in the DTC with a proper CFTC (DTC-CSF1, DTC-CSF2 or DTC-CSF3) than that obtained in the basic DTC. Moreover, the output torque ripple in the DTC with a proper CFTC can be reduced further when a higher triangular frequency is applied. Fig. 12 shows a comparison of the of output torque ripple, from the experimental results, when a step change in the torque reference is applied, in the basic DTC, DTC-CSF1, DTC-CSF2 and DTC-CSF3. To make the comparison fair, the step torque change for each scheme was performed under the same load torque conditions so that the rotor speed operated at around 370 rpm. From the figure, it can be seen that the largest torque ripple is produced with the hysteresis-based DTC.

To reduce the torque ripple, the CFTC is utilized, and as

TABLE III
PI CONTROLLER GAINS AND CROSSOVER FREQUENCY.

Schemes	PI Controller gains		Crossover freq.
	K_p	K_i	f_c (kHz)
DTC-CSF1	29	9937.5	0.719
DTC-CSF2	34.9	11925	0.86
DTC-CSF3	52.3	17887	1.3

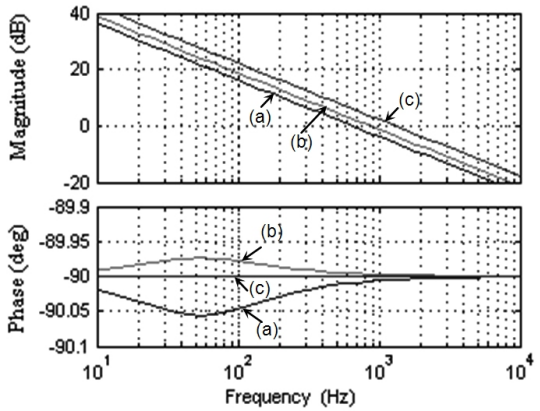

Fig. 10. Bode plot of loop gain with PI controller for (a) DTC-CSF1, (b) DTC-CSF2 and (c) DTC-CSF3.

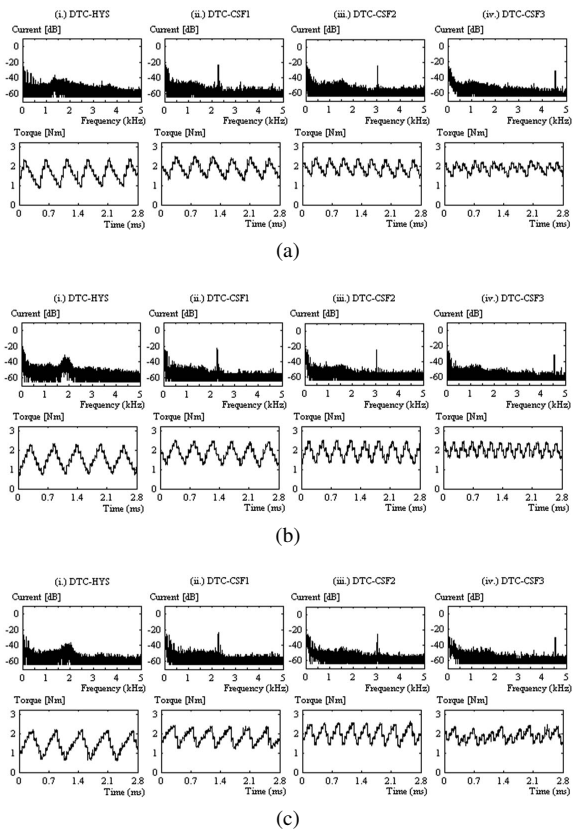

Fig. 11. Experimental results of phase current frequency spectrum and output torque for the basic DTC, DTC-CSF1, DTC-CSF2 and DTC-CSF3 at the speed about (a) 20 rad/s (b) 30 rad/s and (c) 55 rad/s.

mentioned earlier, the output torque can be reduced further when a higher triangular frequency is applied. Obviously, the output torque ripple in the DTC-CSF3 is greatly reduced with a constant and the highest switching frequency. The generated waveforms of the upper triangular for each different frequency (as shown in Fig. 12) can be clearly seen by using a larger scale as depicted in Fig.13.

Finally, to verify the proper operation of the CFTC in regulating the output torque, a square-wave speed command is applied to the basic DTC and the DTC-CSF2. The waveforms of the output torque, the rotor speed (measured from a speed sensor) and the d-axis stator flux for each scheme are as shown in Fig. 14. From this figure, it can be seen that, the dynamic

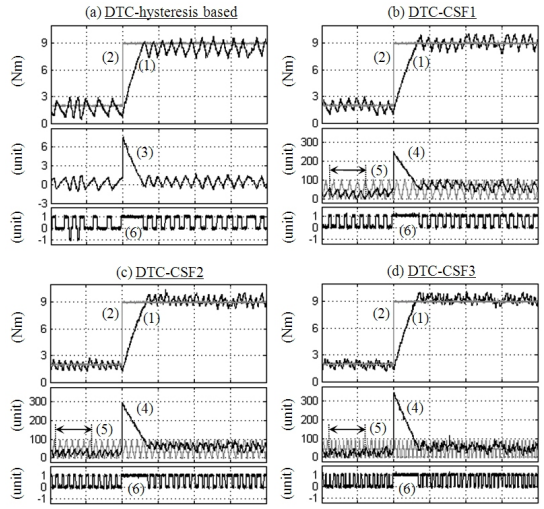

Fig. 12. Experimental results for step response of torque in (a) DTC-hysteresis based, (b) DTC-CSF1, (c) DTC-CSF2 and (d) DTC-CSF3. (1) is output torque, (2) is reference torque, (3) is torque error, (4) is output of PI controller, (5) is upper triangular waveform, (6) is torque error status. (x-axis or time scale: 2 ms/div.)

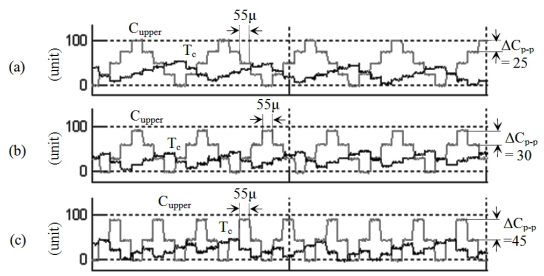

Fig. 13. The zoomed image (zoomed area indicated by '↔) of the waveforms of upper triangular and output of PI controller for (a) DTC-CSF1, (b) DTC-CSF2 and (c) DTC-CSF3, corresponds the results obtained in Fig. 12 (b),(c) and (d). (Time scale: 1 ms/div.)

torque and the speed profiles are comparable to those of the hysteresis-based DTC, but, with the added advantages of a reduced torque ripple and a constant switching frequency.

VI. Conclusions

This paper suggests a simple way to provide a high constant switching frequency and hence reduce torque ripple, by replacing the torque hysteresis controller with a CFTC in the basic DTC structure. The paper showed that with a limited sampling frequency, the carrier frequency utilized in a CFTC can be increased further to its maximum (which is at one-quarter of the maximum sampling frequency). Some experimental results were presented to show that a significant reduction in the output torque ripple can be achieved with the proper PI-controller gains and the proper selection of a triangular frequency in CFTC.

Acknowledgment

The authors would like to thank the Ministry of Science, Technology and Innovation (MOSTI), the Universiti Teknikal Malaysia Melaka (UTeM) and the Universiti Teknologi Malaysia (UTM) for providing the funding and sponsorship for this research.

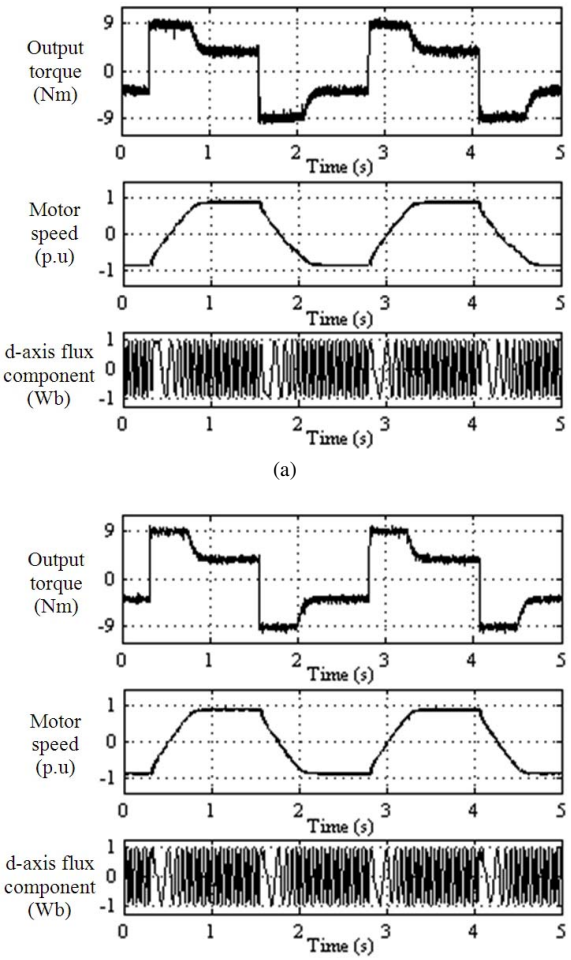

Fig. 14. Experimental results of output torque, motor speed and d-axis flux component for a square-wave speed reference for (a) the basic DTC and (b) DTC-CSF2 based induction machine drives.

References

[1] I. Takahashi and T. Noguchi, "A new quick-response and high-efficiency control strategy of an induction motor," *IEEE Trans. Ind. Appl.*, Vol. IA-22, No. 5, pp. 820-827, Sep. 1986.

[2] T. Noguchi, M. Yamamoto, S. Kondo, and I. Takahashi, "Enlarging switching frequency in direct torque-controlled inverter by means of dithering," *IEEE Trans. Ind. Appl.*, Vol. 35, Np. 6, pp. 1358-1366, Nov./ Dec. 1999.

[3] J. W. Kang and S. K. Sul, "Analysis and prediction of inverter switching frequency in direct torque control of induction machine based on hysteresis bands and machine parameters," *IEEE Trans. Ind. Eletron.*, Vol. 48, No. 3, pp. 545-553, Jun. 2001.

[4] D. Casadei, G. Serra, and A. Tani, "Analytical investigation of torque and flux ripple in DTC schemes for induction motors," in proc. of IECON 97, Vol. 2, pp. 552-556, 1997.

[5] J. K. Kang, D. W. Chung, and S. K. Sul, "Direct torque control of induction machine with variable amplitude control of flux and torque hysteresis bands," *International Conference in Electric Machines and Drives*, pp. 640-642, 1999.

[6] T. G. Habetler, F. Profumo, M. Pastorelli, and L. M. Tolbert, "Direct torque control of induction machines using space vector modulation," *IEEE Trans. Ind. Appl.* Vol. 28, No. 5, pp. 1045-1053, Sep./Oct. 1992.

[7] J. K. Kang and S. K. Sul, "Torque ripple minimization strategy for direct torque control of production motor," *IAS Annual Meeting in Industry Applications Conference*, Vol.1, pp. 438-443, 1998.

[8] S. Mir and M. E. Elbuluk, "Precision torque control in inverter-fed induction machines using fuzzy logic," *26th Annual IEEE Power Electronics Specialists Conference*, Vol.1, pp. 396-401, 1995.

[9] I. G. Bird and H. Zelaya De La Parra, "Fuzzy logic torque ripple reduction for DTC based AC drives," *Electronics Letters*, Vol. 33, pp. 1501-1502, 1997.
[10] D. Casadei, G. Serra, and A. Tani, "Improvement of direct torque control performance by using a discrete SVM technique," *29th Annual IEEE Power Electronics Specialists Conference*, Vol.2., pp. 997-1003, 1998.
[11] N. R. N. Idris and A. H. M. Yatim, "Direct torque control of induction machines with constant switching frequency and reduced torque ripple," *IEEE Trans. Ind. Eletron.*, vol. 51, No. 4, pp. 758-767, Aug. 2004.
[12] A. Jidin, M. Basar, A. Noordin, N. Idris, and A. Yatim, "A wide-speed high torque capability utilizing overmodulation strategy in DTC of induction machines with constant switching frequency controller," *International Conference on Power Electronics and Drive Systems*, pp. 649-654, 2009.
[13] C. Lascu, I. Boldea, and F. Blaabjerg, "A modified direct torque control for induction motor sensorless drive," *IEEE Trans. Ind. Appl.*, Vol. 36, No. 1, pp. 122-130, Jan./Feb. 2000.
[14] A. Tripathi, A. M. Khambadkone, and S. K. Panda, "Torque ripple analysis and dynamic performance of a space vector modulation based control method for AC-drives," *IEEE Trans. Power Eletron.*, Vol. 20, No. 2, pp. 485-492, Mar. 2005.
[15] Y.-S. Lai and J.-H. Chen, "A new approach to direct torque control of induction motor drives for constant inverter switching frequency and torque ripple reduction,", *IEEE Trans. Energy Convers.*, Vol. 16, No. 3, pp. 220-227, Sep. 2001.
[16] G. Papafotiou, J. Kley, K. G. Papadopoulos, P. Bohren, and M. Morari, "Model predictive direct torque control;part II: implementation and experimental evaluation," *IEEE Trans. Ind. Eletron.*, Vol. 56, No.6, pp. 1906-1915, Jun. 2009.
[17] J. Beerten, J. Verveckken, and J. Driesen, "Predictive direct torque control for flux and torque ripple reduction," *IEEE Trans. Ind. Eletron.*, Vol. 57, No.1, pp. 404-412, Jan. 2010.
[18] T. Geyer, G. Papafotiou, and M. Morari, "Model predictive direct torque control;part I: concept, algorithm, and analysis," *IEEE Trans. Ind. Eletron.*, Vol. 56, No.6, pp. 1894-1905, Jun. 2009.

Auzani Jidin received his B.Eng. and M.Eng. in Power Electronics and Drives from the Universiti Teknologi Malaysia (UTM), Johor, Malaysia in 2002 and 2004, respectively. He is currently pursuing his PhD at the same university. He is a Lecturer in the Department of Power Electronics and Drives, Faculty of Electrical Engineering, Universiti Teknikal Malaysia Melaka (UTeM), Malaysia. His research interests include the field of power electronics, motor drive systems, field programmable gate arrays (FPGA) and digital signal processing (DSP) applications.

Nik Rumzi Nik Idris received his B.Eng. in Electrical Engineering from the University of Wollongong, Wollongong, Australia, his M.Sc. in Power Electronics from Bradford University, Bradford, West Yorkshire, U.K., and his Ph.D. from the Universiti Teknologi Malaysia, Skudai, Malaysia, in 1989, 1993, and 2000, respectively. He was a Visiting Research Associate at the University of Akron, Akron, OH, in 2002. Currently, he is an Associate Professor at the Universiti Teknologi Malaysia, and an Administrative Committee Member of the Industry Applications Societies (IAS)/Power Electronics (PELS)/Industrial Electronics (IES) Joint Chapter of the IEEE Malaysia Section. His research interests include ac drive systems and DSP applications in power electronic systems.

Abdul Halim Mohd Yatim received his B.Sc. in Electrical and Electronic Engineering from Portsmouth Polytechnic, Portsmouth, U.K., in 1981, and his M.Sc. and Ph.D. in Power Electronics from Bradford University, Bradford, U.K., in 1984 and 1990, respectively. Since 1982, he has been a member of the faculty at the Universiti Teknologi Malaysia, Johor, Malaysia, where he is currently a Professor and the Deputy Dean of the Faculty. He has been involved in several research projects in the areas of power electronic applications and drives. He was a Commonwealth Fellow from 19941995 at Heriot-Watt University, Edinburgh, U.K., and a Visiting Scholar at the Virginia Power Electronics Center, Virginia Polytechnic Institute and State University, Blacksburg, in 1993. Dr. Yatim is a Corporate Member of the Institution of Engineers Malaysia. He is a Registered Professional Engineer with the Malaysian Board of Engineers. He currently holds the Interim Chapter Chair of the Malaysian Section of the IEEE Industrial Electronics/Industry Applications/Power Electronics Joint Societies.

Tole Sutikno received his B.Eng. in Electrical Engineering from Diponegoro University (UNDIP), Semarang, Indonesia and his M.Eng. in Power Electronics from Gadjah Mada University UGM), Yogyakarta, Indonesia, in 1999 and 2004, respectively. Since 2001 he has been a Lecturer in Electrical Engineering Department, Universitas Ahmad Dahlan (UAD), Yogyakarta, Indonesia. Currently, he is pursuing his PhD. in the Energy Conversion Department, Universiti Teknologi Malaysia (UTM), Johor, Malaysia. His research interests include the field of power electronics, motor drive systems and field programmable gate array (FPGA) applications.

Malik E. Elbuluk received his B.Sc. (with honors) from the University of Khartoum, Khartoum, Sudan, and his M.S., E.E., and D.Sc. from the Massachusetts Institute of Technology (MIT), Cambridge, in 1976, 1980, 1981, and 1986, respectively, all in Electrical Engineering. He is currently a Professor at the University of Akron, Akron, OH, where he has been since 1989. He was with the faculty of the Electrical and Computer Engineering Department and the Electric Power Research Center, North Carolina State University, from 1986 to 1989. He was a Summer Research Fellow at the NASA Lewis Research Center, Cleveland, OH, from 1991 to 2000. His work at NASA included low-temperature electronics for space missions, modeling and simulation of the Space Station Freedom (SSF), power by wire (PBW), power electronic building blocks (PEBB), starters/generators for aircraft engines and the sensorless control of electromechanical actuators (EMA) for the more electric aircraft (MEA). His teaching and research interests include the field of power electronics, electric machines, control systems, fuzzy logic, and neural networks. He is a Registered Professional Engineer in the State of Ohio.